International Journal of Greenhouse Gas Control 119 (2022) 103700

Contents lists available at ScienceDirect

International Journal of Greenhouse Gas Control

journal homepage: www.elsevier.com/locate/ijggc

Top seal assessment of Drake Formation shales for CO_2 storage in the Horda Platform area, offshore Norway

Md Jamilur Rahman [a,*], Manzar Fawad [a], Jens Jahren [a], Nazmul Haque Mondol [a,b]

[a] Department of Geosciences, University of Oslo (UiO), Sem Sælands vei 1, Oslo 0371, Norway
[b] Norwegian Geotechnical Institute (NGI), Sognsveien 72, Oslo 0806, Norway

ARTICLE INFO

Keywords:
Longship
Northern Lights
Aurora
CO_2 storage
Drake Formation
Caprock
Seal quality
Brittleness
Rock physics
Horda platform
Eos

ABSTRACT

Evaluating top seal integrity is crucial for successful subsurface CO_2 storage. Caprock shale geomechanical properties are complex and influenced by various parameters and processes. It is challenging to understand the role of various factors affecting the geomechanical properties; therefore, an integrated approach is required to evaluate top seal shales. In this study, we investigated the caprock properties of the Early Jurassic shaly Drake Formation overlying the reservoir sandstones of Early Jurassic Cook and Johansen formations. The study area is the potential CO_2 storage site Aurora (the Longship CCS project), located in the Horda Platform area, offshore Norway. Based on lithological variations, the Drake Formation is subdivided into upper and lower Drake units. Variations of the geomechanical properties are investigated using wireline logs from 50 exploration wells, two 3D seismic cubes, and several 2D seismic lines. Elastic property-based brittleness indices of the Drake Formation caprock shales are evaluated to identify possible top seal quality. Moreover, seismic attributes and gas leakage scenarios are investigated qualitatively to assess the possibility of injected CO_2 escaping from the reservoir. Low brittleness indices value of the Drake Formation shale near the Aurora injection site indicated that the seal rock might diffuse the injection-related stress change and act as an effective top seal. Based on the integrated qualitative assessment, it is likely that the Drake caprock shale will be acted as an effective top seal in and around the Aurora storage site. However, due to the complex nature of caprock shales, we recommend field-scale numerical simulation to evaluate the injection-induced stress-strain effect.

1. Introduction

Reducing atmospheric greenhouse gas emissions by utilizing geological CO_2 storage (CCS) is necessary to keep global warming below 1.5 to 2°C (Rogelj et al., 2018). CCS is the safest and quickest solution to reduce the emitted CO_2 (Longship-Report, 2020; Peters and Sognnæs, 2019). To realize the importance, the Norwegian Government and Northern Lights - a joint venture company owned by Equinor, Shell, and TotalEnergies, recently initiated a full-scale (capture, transport, and storage) CO_2 storage project 'Longship' in the Horda Platform area, offshore Norway. Northern Lights is the transport and storage component of the Longship project, which includes the capture of CO_2 from the industrial point sources (cement factory and waste-to-energy plant) and then transporting the captured CO_2 (liquefied) by ships to an onshore terminal (Øygarden municipality) on the Norwegian west coast. Finally, the CO_2 will be injected and permanently stored into a deep saline aquifer in the Aurora storage site (31/5-7, Eos well) (~2.6 km below the seabed) by a pipeline (~100 km long; Fig. 1a). Phase 1 includes the capacity to transport, inject and store up to 1.5 Mt of CO_2 per year (Northern Lights, 2022). However, the investments in subsequent phases will be triggered (up to 5 Mt of CO_2 per year) by market demand from large CO_2 emitters across Europe (Northern Lights, 2021). Potential reservoir rocks in the Aurora area are the Cook and Johansen Formation sandstones, and the cap rocks are the Drake and Burton Formation shales belonging to the Early Jurassic Dunlin Group (Fig. 1b). Although several CCS projects worldwide demonstrated safe and reliable CO_2 storage (i.e., Sleipner and Snøhvit in Norway; In Salah in Algeria; Century Plant in the USA; Quest and Aquistore in Canada; etc.), the large scale Longship project (first of its kind) needs further evaluation to assess the potential geomechanical risks.

Reliability of subsurface CO_2 storage depends on caprock integrity and fault sealing potential (Chiaramonte et al., 2015; Park et al., 2020; Rahman et al., 2021, 2020; Rutqvist et al., 2007; Skurtveit et al., 2018). Therefore, caprock characterization is crucial for any CCS project

* Corresponding author.
E-mail address: m.j.rahman@geo.uio.no (M.J. Rahman).

https://doi.org/10.1016/j.ijggc.2022.103700
Received 4 June 2021; Received in revised form 16 May 2022; Accepted 26 May 2022
Available online 30 May 2022

injecting CO_2 into the saline aquifers or depleted hydrocarbon fields. An effective caprock shale has very low matrix porosity and permeability (Chen et al., 2019; Liu et al., 2020; Tan et al., 2019), which prevents upward fluid flow due to high capillary entry pressure (Ingram et al., 1997). It is also unlikely to have caprock failure due to capillary breakthrough because of the low permeability in most shales. Instead, pore-pressure-driven fracturing and fault reactivation are likely scenarios regarding fluid escape/leakage from the storage sites (Bjørlykke et al., 2015; Hansen et al., 2020; Ingram et al., 1997).

Caprock shales significantly vary in composition, porosity, brittleness, heterogeneity, etc. (Storvoll et al., 2005; Mondol et al., 2007; Mondol, 2018). Moreover, shales are deposited under a wide range of conditions and experience post-depositional diagenetic changes during burial (Hart et al., 2013; Bjørlykke et al., 2017). Therefore, shale geomechanical and elastic properties vary considerably as functions of grain size, texture, mineral composition, etc. This phenomenon is evident in the Horda Platform area, where the depositional settings are complex. The paleodepositional conditions of the Drake Formation shales are affected by the structurally influenced sub-basins; hence various properties (Færseth, 1996; Steel and Ryseth, 1990; Steel, 1993). In addition to the variations of depositional conditions, mineralogical changes, and diagenetic history (e.g., mechanical versus chemical compaction), exhumation of the study area (Baig et al., 2019; Rahman et al., 2020) are also influenced the Drake Formation shale caprock properties.

Failure behavior of caprock shales may vary due to variations in their petrophysical, acoustic, elastic, and geomechanical properties. Shear failure or tensile fracturing occurs when the shear stress exceeds the shear strength. This type of failure is controlled by the brittleness indices property of the caprock, where the brittle caprock fails relatively quickly than the ductile rock (Nygård et al., 2006). Therefore, it is crucial to characterize shale brittleness property to evaluate caprock integrity. However, the brittleness property, which is also classified as fracability (Holt et al., 2015, 2011; Jin et al., 2014; Rybacki et al., 2016; Wang and Gale, 2009; Yang et al., 2013), is a complex function of rock strength, lithology, texture, effective stress, temperature, fluid type (Handin et al., 1963; Handin and Hager, 1957; Nygård et al., 2006), diagenesis, TOC type, amount and maturation (Walles, 2004; Hansen et al., 2020), natural fractures and other planes of weakness (Gale et al., 2007; Zhang et al., 2016; Johnson et al., 2022), etc. There is no firm definition of the brittleness indices; instead, different quantifying methods have been employed (e.g., Fawad and Mondol, 2021; Grieser and Bray, 2007; Guo et al., 2012; Josh et al., 2012; Kivi et al., 2018; Liu et al., 2020; Mondol et al., 2022; Rickman et al., 2008). All the methods have been estimated to have a range from ductile to brittle, where the more brittle the caprock is, the possibility of failure increases with increasing stresses. The caprock brittleness property also varies significantly at different in-situ stress state conditions (Herwanger et al., 2015). Therefore, for CCS project reliability, a detailed analysis of caprock shale is crucial and needs to be carried out to build confidence in top seal integrity.

The main objective of this study is to characterize the Lower Jurassic Drake Formation caprock shale's properties. The Formation is divided into upper and lower units based on the lithology, where the upper unit consists of heterolithic deposits comprising sandstones with alternating siltstones and claystone. In contrast, the lower unit contained claystone (NPD, 2021). Considering the long-term Longship CCS project goal, this study focuses on the caprock quality of the broader Horda Platform area. A Young's modulus versus Poisson's ratio rock physics template (Perez and Marfurt, 2014; Mondol et al., 2022) is used to evaluate the caprock shale properties. Moreover, two elastic property-based brittleness indices (Fawad and Mondol, 2021; Grieser and Bray, 2007; Rickman et al., 2008) are used to estimate the brittleness property of the Drake Formation caprock shales. Additionally, a seismic attribute-based qualitative assessment is carried out using a cropped 3D seismic volume (Fig. 2) to approximate the caprock properties from seismic. Besides the formation pressure communication, a fault parallel leakage (gas chimney) from the Troll field is used as an analog to discuss the possible seal integrity risks. Moreover, the ranges in elastic properties used in the brittleness indices calculation are improved based on the site-specific wireline log data. Finally, a basin-specific brittleness template has been proposed, which needs further investigation for improved caprock characterization.

2. Materials and methods

In this study, we used wireline logs from 50 exploration wells, two 3D seismic surveys (GN10M1 and GN1101), and several 2D lines (NSR and SG8043 surveys) from the study area (Fig. 2, Table 1) to evaluate the Drake Formation shales caprock properties. As mentioned earlier, the Drake Formation is divided into two units, where the lower unit is shalier than the upper unit. The studied wells are located in various

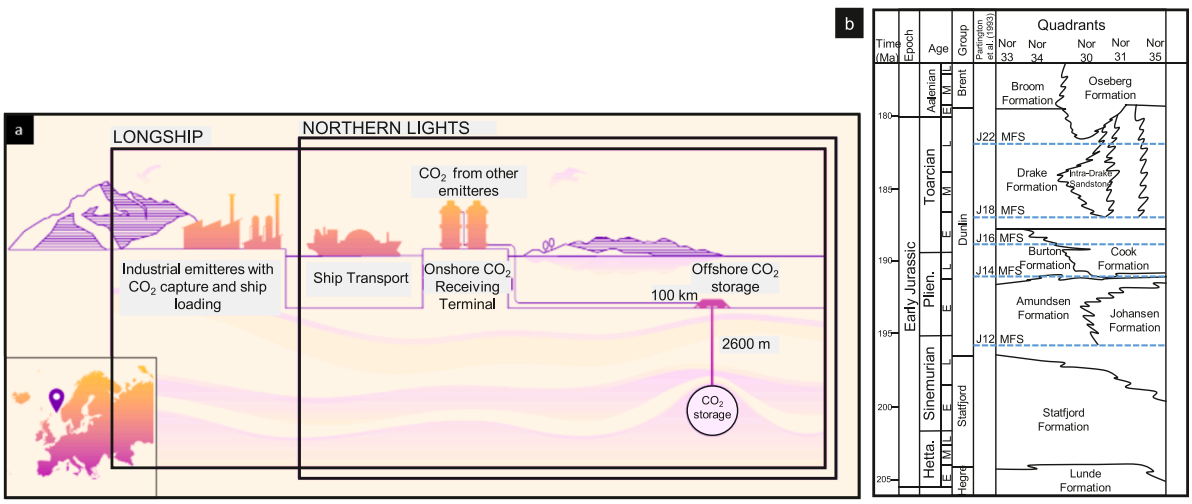

Fig. 1. (a) A schematic representation of the Longship project (courtesy of Northern Lights) shows the location of the Aurora site (inset map) in the Horda Platform area, offshore Norway. The full-scale CCS project includes the capture of CO_2 from Fortum Oslo Varme (Waste incineration plant, Oslo, Norway) and Norcem cement factory (Brevik, Norway) and shipping of captured CO_2 (liquid form) to an onshore terminal (Øygarden) on the Norwegian west coast. The liquified CO_2 will be transported by pipeline to the Aurora site for permanent storage. (b) A generalized Early Jurassic stratigraphic succession of the study area is represented the lithological variation between the different quadrants (modified from Husmo et al. (2003)). MFS is the maximum flooding surface, according to Partington et al. (1993).

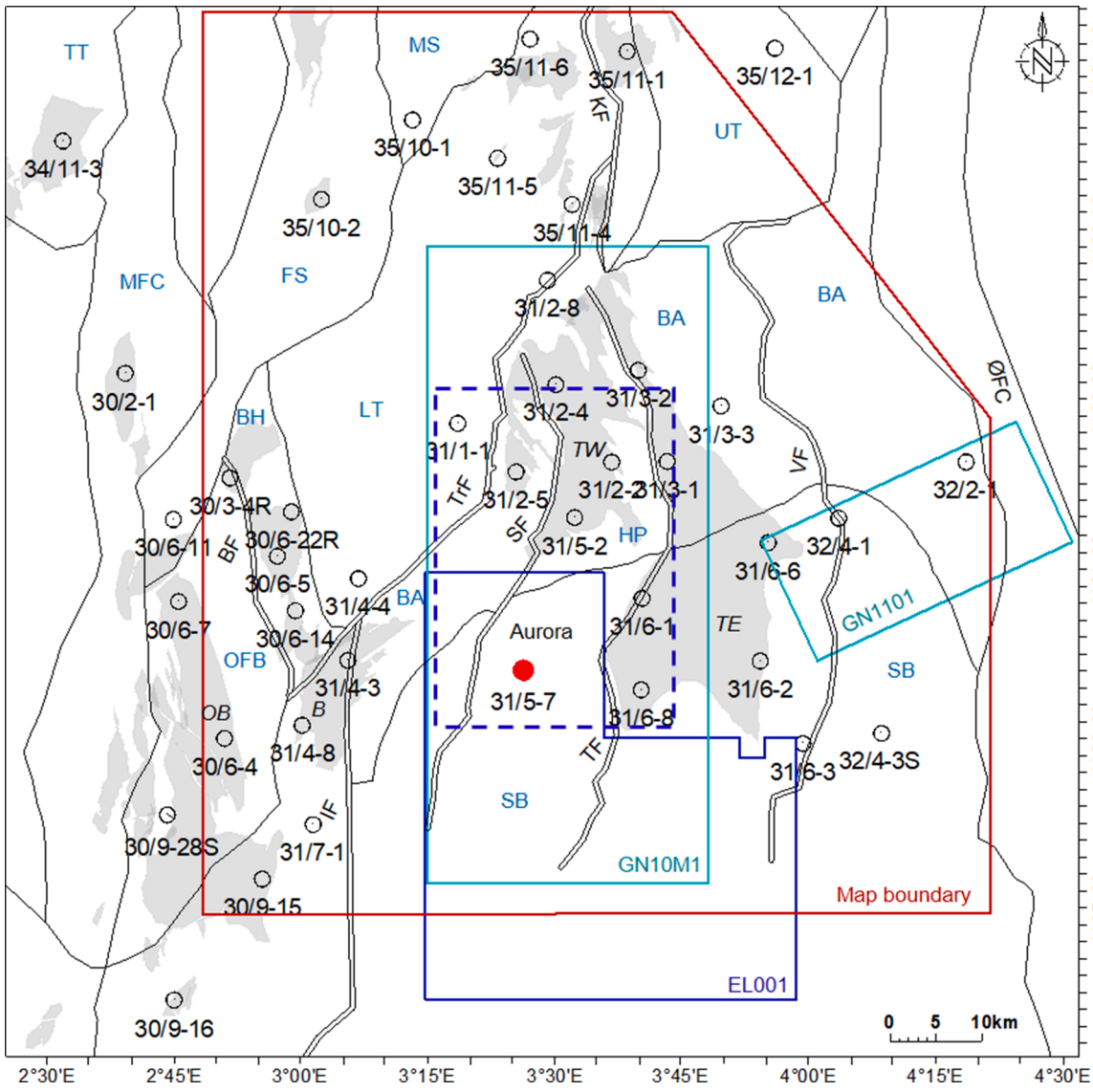

Fig. 2. Map of the study area shows wells (black circles), faults (black lines) and structural elements (e.g., BA = Bjørgvin Arch; BH = Brage Horst; FS = Flatfisk Slope; HP = Horda Platform; LT = Lomre Terrace; MS = Marflo Spur; SB = Stord Basin; TT = Tjalve Terrace; UT = Uer Terrace; Faults: BF = Brage Fault; IF = Idunn Fault; KF = Kinna Fault; MFC = Mokkurkalve Fault Complex; OFB = Oseberg Fault Block; TF = Tusse Fault; TrF = Troll Fault; ØFC = Øygarden Fault Complex). Grey shaded polygons illustrate the hydrocarbon fields and discoveries (e.g., B = Brage; OB = Oseberg; TE = Troll East; TW = Troll West) in the study area. The boundary of the regional map is denoted in a red polygon, where the light blue boundaries represent 3D seismic cubes GN10M1 & GN1101. For Aurora site-specific evaluation, the cropped 3D volume (dotted blue polygon) is used. The first CCS license (EL001) in offshore Norway is indicated by blue polygon, where the red filled circle is the proposed CO_2 injection well Eos (31/5-7).

structural settings defined by the Norwegian Petroleum Directorate (NPD) and represent different present-day top Drake caprock depth ranges (Fig. 2; Table 1). The majority of the studied wells (a total of 16) are from the Bjørgvin Arch (BA), while a considerable number of wells are also used from Stord Basin (SB), Lomre Terrace (LT), Oseberg Fault Complex (OFC), and Brage Horst (BH). The remaining wells are from Flatfisk Slope (FS), Uer Terrace (UT), Mokkurkalve Fault Complex (MFC), Tjalve Terrace (TT), and Marflo Spur (MS) (Fig. 2, Table 1). According to NPD (2021), the Cook and Johansen formation sandstones encountered by the studied wells are water wet.

Because of the complex nature of caprock shale properties, an integrated workflow is implemented to characterize the top seal effectiveness (Fig. 3). Although Drake caprock shale from the Aurora injection site is analyzed as an example in this study, this integrated workflow can be useful in any potential CO_2 storage sites top seal evaluation. After quality control, the wireline logs are used to conduct petrophysics and rock physics analyses. Several well's average property maps and Young's Modulus-Poisson's Ratio (E-PR) cross plots have been generated to characterize the caprock shales. Simultaneously, seismic interpretation and seismic attributes analyses are carried out, mainly focusing on the area surrounding the Eos injection well (31/5-7). Possible top seal integrity risks, such as the presence of faults and fractures, fault leakage possibility, etc., are evaluated from the seismic-based analysis. Finally, we evaluated the top seal geomechanical properties and integrity by incorporating all the results.

Rock properties such as Young's modulus (E) and Poisson's ratio (PR) are proxies of rock stiffness and represent the geomechanical property under stress. These properties are calculated using compressional wave velocity (V_p), shear wave velocity (V_s), and bulk density (ρ) logs. However, the V_s used in this study is not acquired but predicted using Random Forest (RF), a machine learning algorithm. We tested several machine learning algorithms (i.e., RF, kNN, NN), and the results are compared with the acquired V_S (Fig. 4a). The Random Forest (RF) method, which showed a correlation nearly as good as Neural Network

Table 1
Well Database with structural elements, Drake caprock shales present/maximum burial depth and thickness (adapted from Rahman et al. (2022).

Well name	Structural Elements (NPD)	Upper Drake (m BSF)		Thickness (m) *Upper Drake*	Lower Drake (m BSF)		Thickness (m) *Lower Drake*
		Present	Paleo*		Present	Paleo*	
30/9-15	Bjørgvin Arch	2147	2327	78	2226	2406	107
30/9-16		2879	3044	100	2980	3145	81
30/12-1		2998	3133	101	3099	3234	97
31/2-1		1577	1697	86	1663	1783	56
31/2-2		1701	1831	57	1759	1889	47
31/2-3		1542	1932	68	1611	2001	39
31/2-4		1541	1801	58	1600	1860	46
31/2-5		1705	1945	66	1772	2012	64
31/3-1		1458	1838	71	1530	1910	57
31/3-2		1586	1906	83	1669	1989	-
31/3-3		1850	2370	49	1900	2420	47
31/4-3		2216	2386	59	2275	2445	72
31/4-8		1936	2076	69	2006	2146	66
31/5-2		1693	1883	79	1772	1962	61
31/7-1		2307	2517	81	2388	2598	69
35/11-7		2162	2357	64	2227	2422	40
31/5-7	Stord Basin	2172	2522	74	2247	2597	53
31/6-1		1507	1837	76	1584	1914	52
31/6-2		1649	2109	47	1697	2157	31
31/6-3		1647	2077	35	1683	2113	32
31/6-6		1708	2178	47	1756	2226	30
31/6-8		1640	1970	98	1739	2069	62
32/4-1		1304	2004	43	1348	2048	49
31/1-1	Lomre Terrace	2198	2398	84	2282	2482	42
31/2-8		2351	2581	61	2413	2643	41
31/4-4		2558	2558	71	2630	2630	66
31/2-19S		3272	3472	63	3335	3535	49
35/11-2		3092	3252	74	3167	3327	58
35/11-4		2413	2603	65	2478	2668	37
35/11-5		3014	3194	65	3079	3259	27
35/11-6		3238	3388	85	3323	3473	52
30/3-3	Oseberg Fault Block	2908	3028	58	2966	3086	66
30/3-4R		2759	2884	59	2819	2944	69
30/6-4		2550	2740	94	2645	2835	74
30/6-7		2647	2767	98	2745	2865	91
30/6-19R		2808	2933	49	2858	2983	64
30/9-13S		3259	3259	122	3381	3381	77
30/9-28S		3182	3372	105	3287	3477	73
30/3-2R	Brage Horst	2738	2868	56	2795	2925	67
30/6-5		2775	2915	50	2826	2966	63
30/6-14		2234	2389	60	2295	2450	93
30/6-22R		2796	2901	56	2853	2958	67
31/4-2		2186	2346	68	2255	2415	57
30/6-11	Flatfisk Slope	3415	3505	75	3490	3580	96
35/10-2		3893	4018	62	3955	4080	78
35/11-1	Uer Terrace	2172	2502	59	2231	2561	55
35/12-1		2531	3011	44	2575	3055	-
30/2-1	Mokkurkalve Fault Complex	3636	3701	76	3713	3778	96
34/11-3	Tjalve Terrace	3965	3995	27	3992	4022	36
35/10-1	Marflo Spur	3102	3242	70	3172	3312	37

(NN) has been selected for this study. Moreover, the precedent for using RF for top seal assessment can be viewed in another related study on Draupne and Heather caprock shale evaluation (Rahman et al., 2020). E versus PR cross-plot is used to evaluate the ductility of the Drake caprock shales, where the background template is adapted from Perez and Marfurt (2014). A comparative analysis is also done between the two elastic property-based brittleness indices proposed by Grieser and Bray (2007) and Fawad and Mondol (2021).

A cropped 3D seismic volume from the GN10M1 survey (Fig. 2) is used for Aurora site-specific analysis. Several seismic attributes (i.e., envelope and variance) are generated to assess the spatial variations of lithology, faults, and fractures in and around the Aurora injection site. Seismic attributes analysis is carried out not only for the caprocks but also to evaluate the reservoir quality of the Johansen Formation. The NPD well tops are also updated based on Steel's (1993) sequence stratigraphic concept in the northern North Sea area. The techniques used to estimate brittleness indices and extraction of seismic amplitudes are briefly described below as sub-sections:

2.1. Brittleness indices

Brittleness Indices are the estimations of caprocks' geomechanical property, which depends on many factors such as mineralogy, diagenesis, temperature, pressure, etc. Two elastic property-based brittleness Indices (EBI) methods proposed by Grieser and Bray (2007) and Fawad and Mondol (2021) are used in this study over many other available methods (i.e., Chen et al. 2014, Jin et al. 2014, Rickman et al. 2008, Sharma and Chopra, 2012). The Grieser and Bray (2007) equation is based on the normalization of E and PR and states that:

$$EBI^1 = \frac{1}{2}\left[\frac{E - E_{min}}{E_{max} - E_{min}} + \frac{PR - PR_{max}}{PR_{min} - PR_{max}}\right] \quad (1)$$

where E is static Young's modulus, E_{max} is 69 GPa, E_{min} is 0 GPa, PR is static Poisson's ratio, PR_{max} is 0.5, and PR_{min} is 0. Also, the higher the EBI^1 value is, the more brittle the caprock is. Static E is estimated from P-wave velocity (V_p) using the empirical relation proposed by Horsrud (2001):

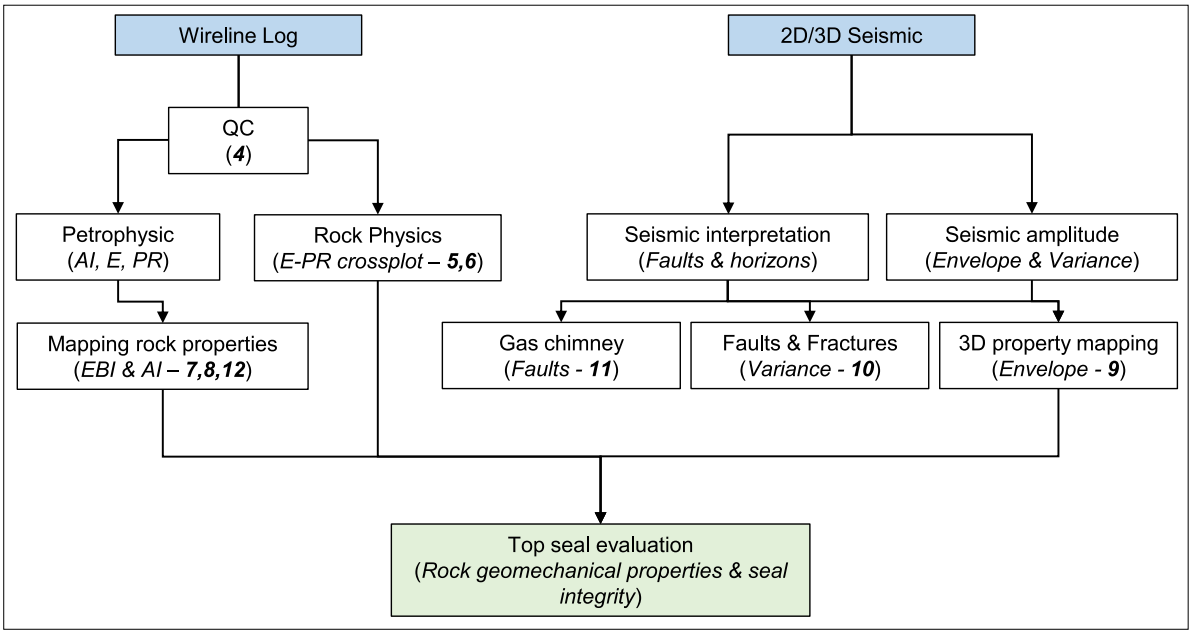

Fig. 3. Illustrated the integrated workflow used in this study to assess the top seal geomechanical properties and integrity in and around the Aurora CO_2 injection site, northern North Sea. Note that bold numeric numbers are represented by figure numbers presented in this study.

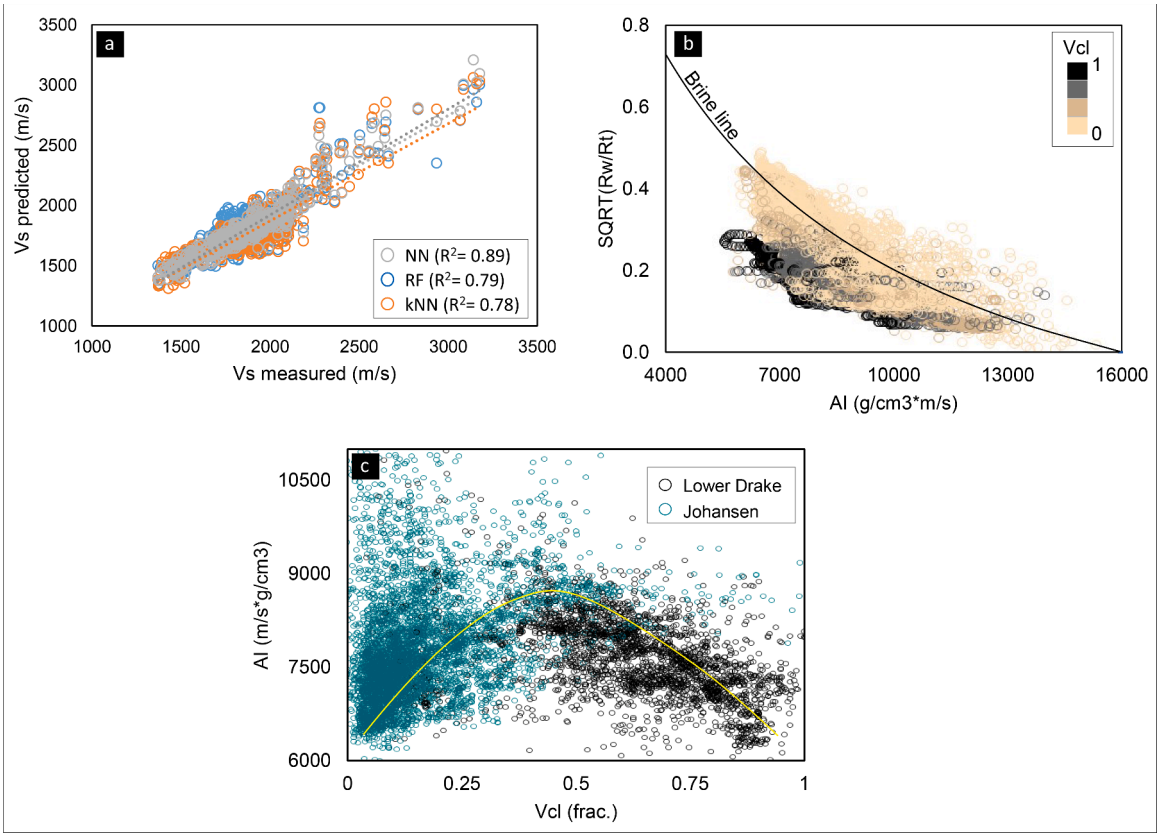

Fig. 4. (a) Comparison between machine learning algorithms estimated Vs with the measured Vs. The Drake Formation data points from well 31/1-1 are used to construct the crossplot (adapted from Rahman et al. (2022)). (b) The pore water resistivity is estimated from seven wells taken from the Drake and Johansen formations color-coded by the volume of clay (Vcl) covering various depths in the study area, which are calibrated with the brine line. Several Rw values are tested until a better match is observed between the data points and the brine line using Rw = 0.08, (c) Data points from 7 wells located within the studied 3D seismic volume (outline in Fig. 2) show the acoustic impedance variations due to clay volume changes in lower Drake unit and Johansen Formation. Marion et al. (1992) explained the inverted V-shape behavior for sand-clay mixture is visible for sandy Johansen Formation and clayey lower Drake unit data.

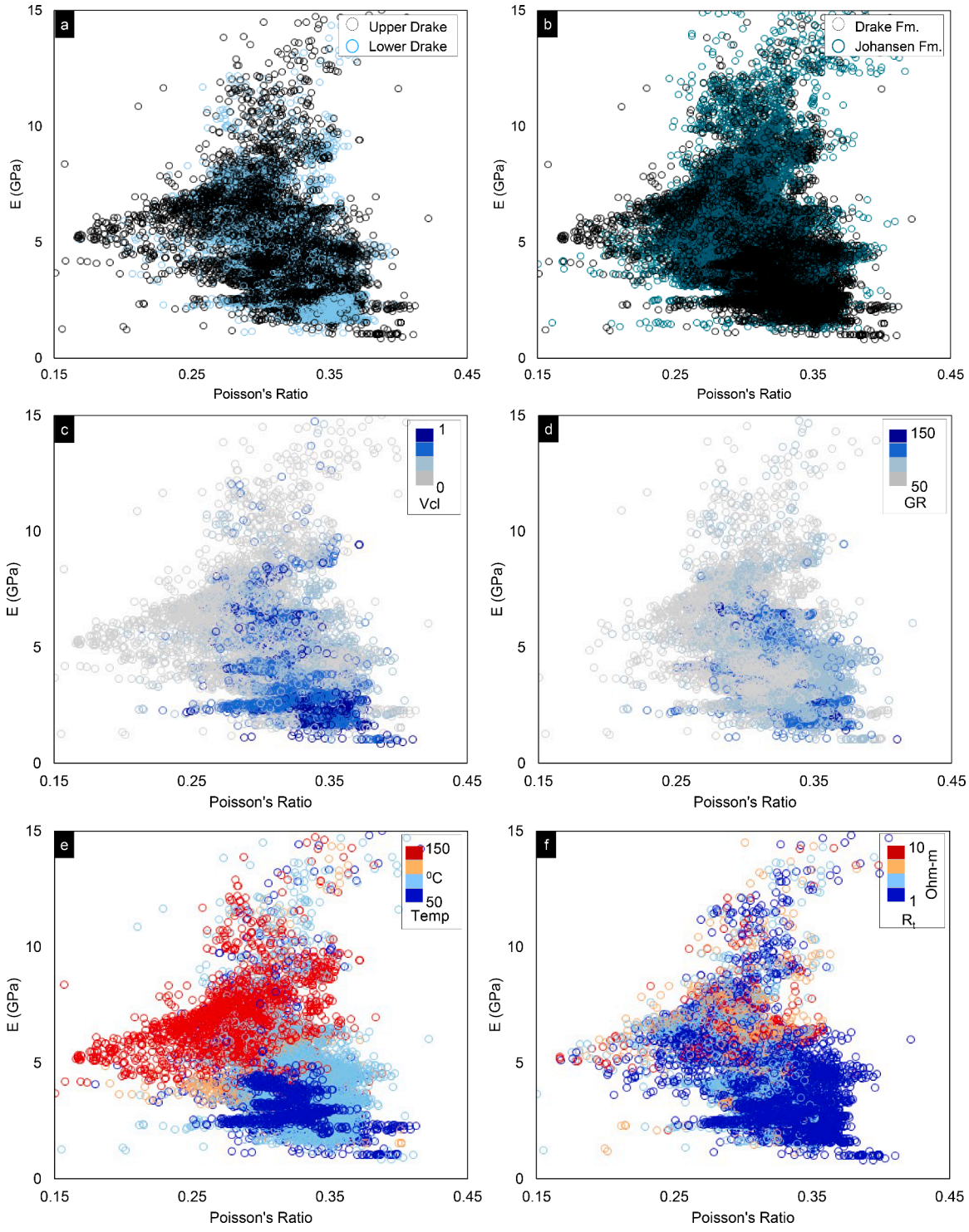

Fig. 5. Cross-plots of E versus PR for (a) the upper and lower units of the Drake Formation shales, and (b) the entire Drake and Johansen Formations illustrate the variation between them. The volume of clay (c), and gamma-ray (d) of the Drake Formation represent the depositional variation. The maximum temperature corrected for exhumation (e), and deep resistivity of both units are demonstrated the diagenetic effect on caprock shale.

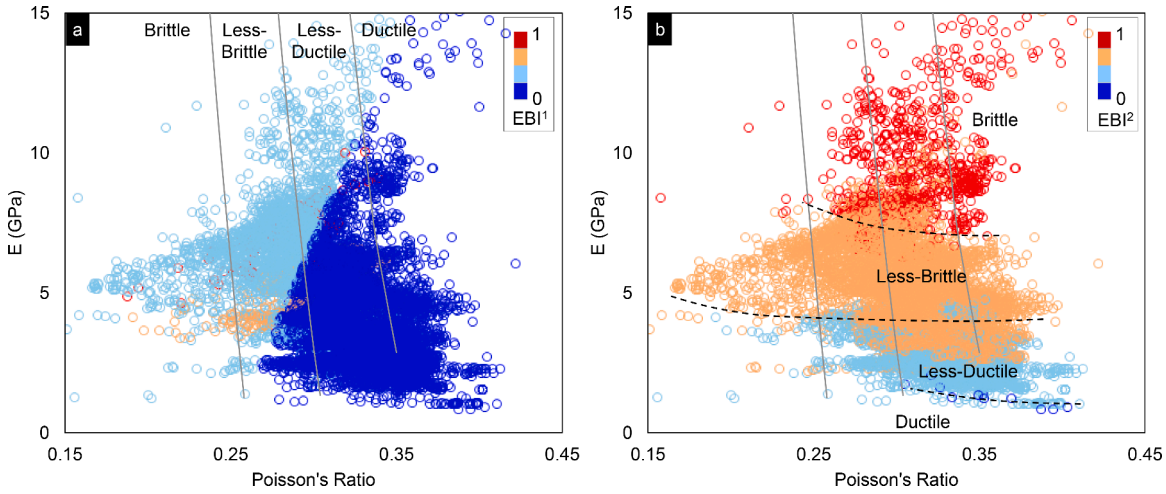

Fig. 6. Cross-plots of E versus PR data points from the Drake Formation color-coded with EBI1 (a) and EBI2 (b). The background curves are adapted from Perez and Marfurt (2014). The dotted lines are proposed new templates based on the EBI2 property range.

$$E = 0.076V_p^{3.23}, \tag{2}$$

Where V_p is in km/s. The PR (dynamic = static) is calculated from V_p and V_s using the equation below:

$$PR = \frac{V_p^2 - 2V_s^2}{2\left(V_p^2 - V_s^2\right)}, \tag{3}$$

The other EBI equation used in this study proposed by Fawad and Mondol (2021) is based on acoustic impedance (AI) and deep resistivity (R_t) and is defined as:

$$EBI^2 = \frac{\frac{AI}{V_{Pom}} - \rho_{om} - \sqrt{\frac{aR_w}{R_t}}\left[AI\left(\frac{1}{V_{Pw}} - \frac{1}{V_{Pom}}\right) - (\rho_w - \rho_{om})\right]}{\left[(\rho_{ma} - \rho_{om}) - AI\left(\frac{1}{V_{Pma}} - \frac{1}{V_{Pom}}\right)\right]}, \tag{4}$$

where V_{Pma} and V_{Pw} are the P-wave velocities of the mineral matrix and the pore fluid (water), respectively, V_{Pom} is the P-wave velocities of the organic matter (OM), r_{om} is the density of organic matter, r_{ma} is the density of mineral grains, r_w is the density of pore fluids (water in this case), R_t is formation resistivity, R_w is the resistivity of water (0.08 based on estimates from the well calibration shown in Fig. 4b), 'a' is tortuosity factor, and AI is acoustic impedance. The tortuosity factor 'a' controls the slope of the water-matrix curved line and can be selected in a zone depending on pore structure, grain size, and level of compaction. Here, brittleness is defined as an increase in the stiffness of the rock due to compaction and the percentage of stiff minerals (quartz, carbonate, and dolomite). The equation is based on the physical and elastic properties of three end-member materials (organic matter, quartz, clay/water).

2.2. Seismic attributes

Seismic attributes provide a qualitative assessment of the subsurface's geometry and physical parameters and are the principal factor determining the elastic properties (i.e., acoustic impedance, reflection coefficient, velocities, absorption, etc.). Due to the relation between these parameters and geological patterns and features (i.e., structural configuration, lithological variation, fluid content, etc.), it is possible to quantify rock and fluid properties from seismic attributes (Chopra and Marfurt, 2005). Attributes can be generated using both pre-stack and post-stack seismic data. In this study, we only considered post-stack attributes generated by the Petrel-2019 volume attribute function. Seismic attribute analysis focused only on the Aurora injection site (Eos well), where a cropped 3D volume (outline in Fig. 2) from the GN10M1 survey is used. Although stacking processes eliminates offset and azimuth-related information, the post-stack attributes are suitable for observing large amounts of data in initial reconnaissance investigations (Taner, 2001). In this study, a post-stack attribute known as the envelope is used, which is proportional to the acoustic impedance contrast (Barnes, 1991; Cohen, 1995). The envelope attribute, also known as instantaneous amplitude (reflectivity), is the total instantaneous energy of the analytical signal within a defined window (i.e., length: 33). The reflection might vary due to possible gas accumulation, tuning effect, depositional environments, spatial porosity changes, or other lithological variations. Another post-stack attribute called 'variance' is used for faults and fracture identification. The variance property is estimated using the filter 3, 3, 15 inline, crossline number of traces, and vertical smoothing, respectively. No dip correction has been applied. Variance attribute can isolate edge, which means horizontal discontinuity of amplitude caused by faults and fractures. Moreover, time structure surfaces (i.e., Lower Drake and Johansen formations) are interpreted and used to estimate the average attribute properties for individual layers. The time structure maps are generated by interpreting the full fold post stacked 3D seismic volume GN10M1.

Generally, a correlation between seismic properties (e.g., AI, V_p) and petrophysical parameters (e.g., porosity, V_{cl}) has been evident. For instance, low acoustic impedance (AI) is associated with high porosity or vice versa (Pablo, 2004), or clean sand or shale show relatively low AI compared to sediments with mixed grain sizes. A similar trend is observed in wireline log data from the seven wells within the analyzed cropped seismic volume. The main caprock shale (lower Drake unit) and reservoir sandstone (Johansen Formation) data are shown in Fig. 4c. Overall, Johansen Formation shows a positive increasing trend between AI and V_{cl}, while the Lower Drake represents a negative correlation

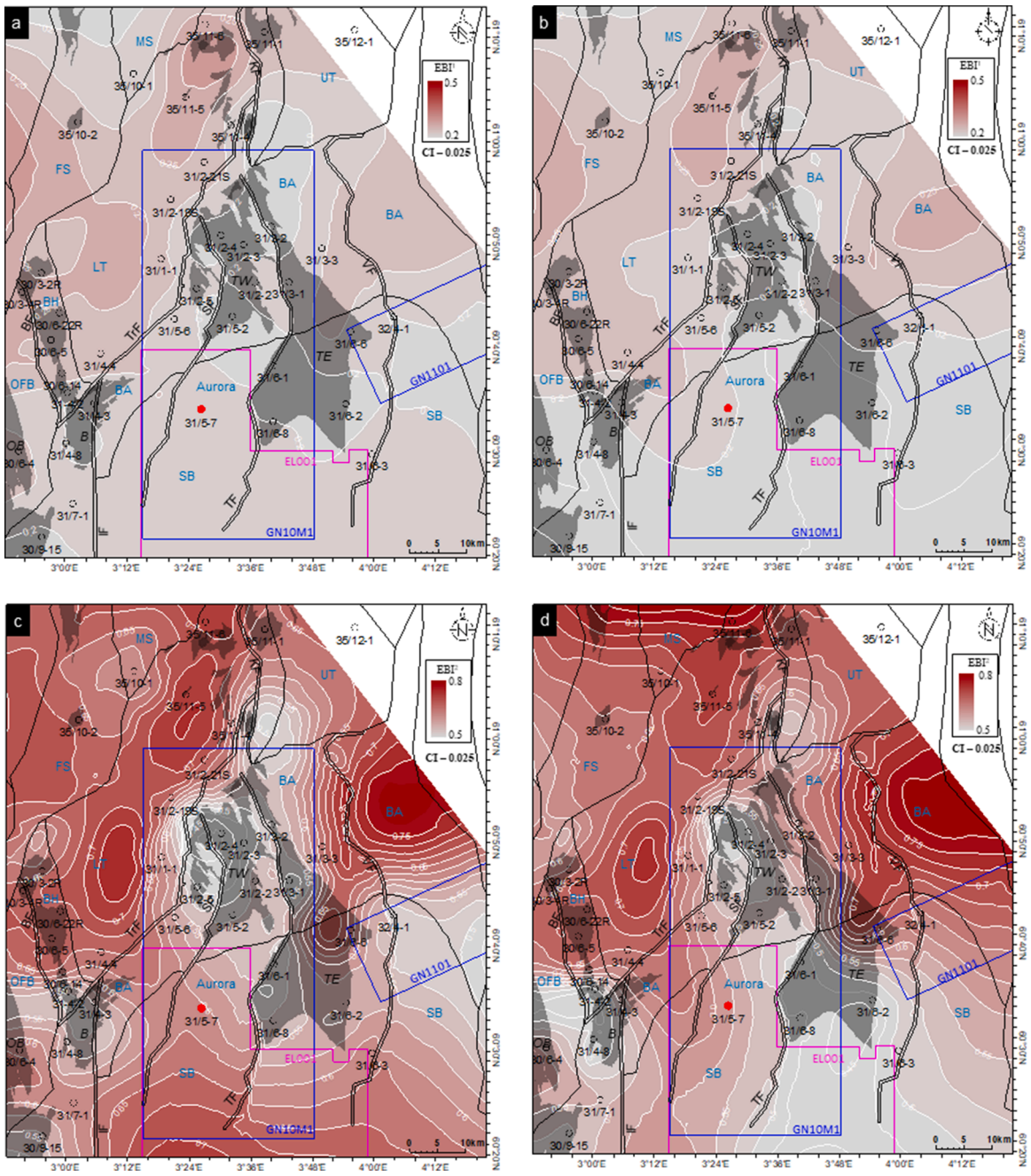

Fig. 7. Wells averaged elastic property-based brittleness indices maps of upper Drake (a & c), and lower Drake (b & d) units estimated using the equation proposed by Grieser and Bray (2007) (a & b), and Fawad and Mondol, 2021 (c & d). The maps represent the spatial variation of caprock stiffness in both methods. Note that the maps have different color scales. Also, EBI2 well average data were presented by Rahman et al. (2022) for different purposes.

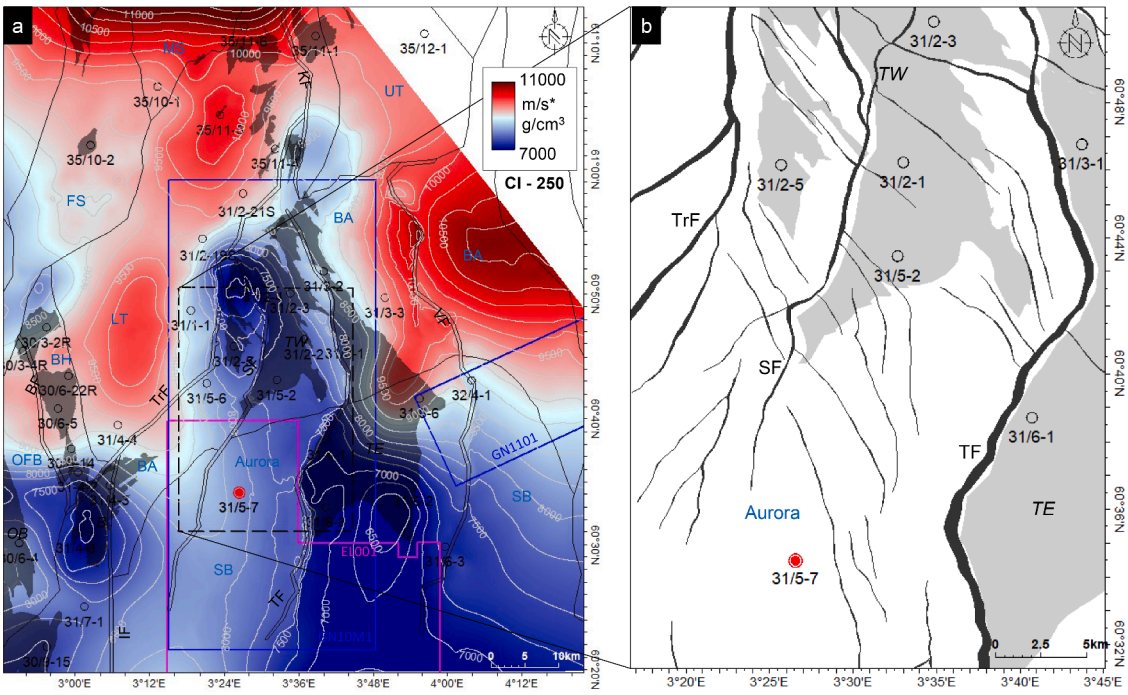

Fig. 8. The acoustic impedance (average value calculated for each well) map of the lower Drake unit shows the spatial variation of AI (a). The cropped 3D seismic volume map shows faults, injection (31/5-7), and other wells (31/5-2, 31/2-1, and 31/2-3) and Troll fields as reference (b).

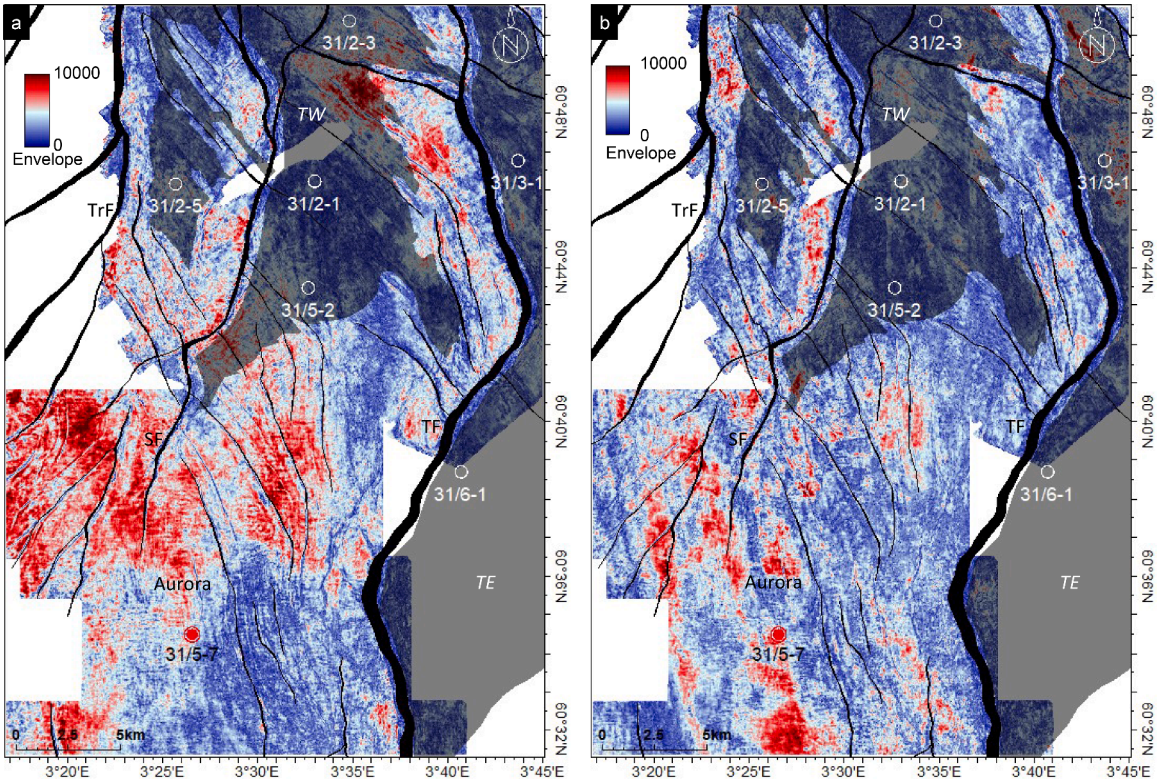

Fig. 9. The envelope attribute is estimated from post-stack cropped 3D seismic volume representing the average properties of lower Drake unit (a) and Johansen Formation (b). The major and minor faults, studied wells, and the hydrocarbon-producing Troll Field are shown as a references.

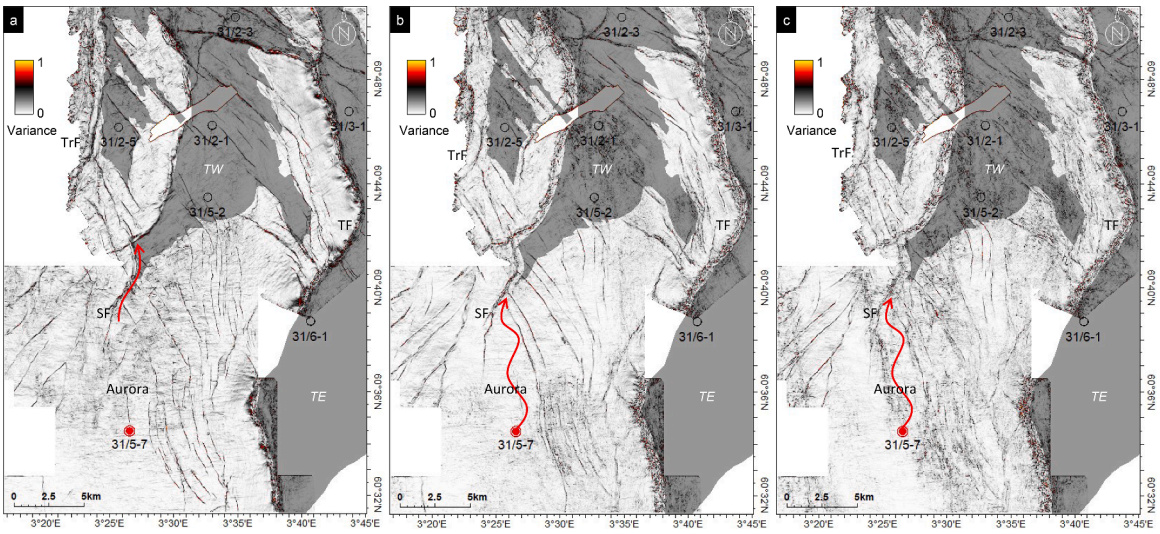

Fig. 10. The variance attribute shows the possible faults and fractures on top of Sognefjord Formation (a), Lower Drake unit (b), and top Johansen Formation (c). The red circle shows the location of the injection well (31/5-7), and the red arrow indicates the possible CO_2 migration path.

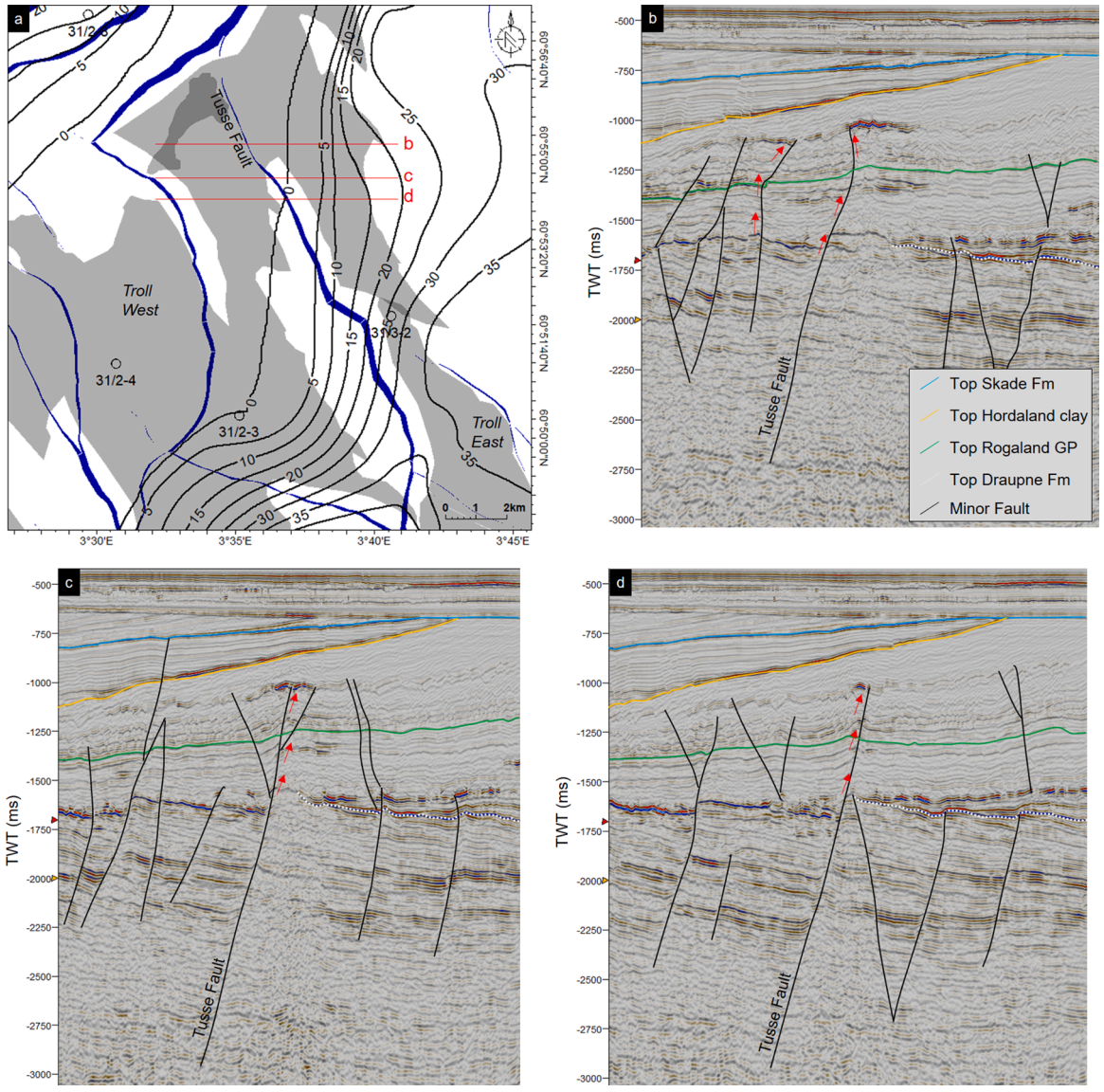

Fig. 11. The map represents the Tusse fault which separates Troll east and Troll west Gas Fields (a). The locations of seismic cross-sections (b, c & d) are shown with the Draupne Formation (primary caprock) thickness contour (Rahman et al., 2020). The possible gas chimney in block 31/2 is interpreted in the Tusse fault zone where the primary caprock is not present. High amplitude in the tipping point of the Tusse fault indicated possible vertical gas leakage (red arrows), which accumulated within the Hordaland clay.

(decreasing AI with increasing V_{cl}). The trend roughly follows the inverted V-shape behavior of the sand-shale mixture proposed by Marion et al. (1992). The higher the AI, the less sorted the rocks are.

3. Results

3.1. Caprock properties

The studied Drake caprock shales geomechanical property is characterized in Young's modulus (E) versus Poisson's ratio (PR) crossplots (Fig. 5). Data from the upper and lower Drake units follow a similar trend where E ranges between 0 and 15 GPa and PR ranges between 0.17 and 0.41. The Johansen Formation reservoir sandstone data points are also illustrated for comparison, which reveals more or less similar properties to the Drake caprock Formation (Fig. 5b). Gamma-ray is generally used as a proxy for depositional variation. However, the Drake Formation E and PR values do not show separate clusters; instead, mixed data clustering is observed. In the temperature plot, a gradual increase of E with increasing temperature is identified (Fig. 5e). Because of the exhumation effect in the study area, maximum (paleo) temperature has been estimated using the exhumation corrected paleo-depth experienced by the studied intervals (Rahman et al., 2022). 100 °C demarcated a transition based on the maximum temperature where the lower temperature cluster represents low E accompanied by higher PR. On the contrary, higher temperature data points illustrated the opposite (higher E and lower PR). Few data points show high deep resistivity (R_t) values fall in the high-temperature cluster (Fig. 5f). However, most of the data points with low R_t are distributed randomly without any specific trend.

The elastic property-based brittleness Indices (BI) such as EBI^1 (Eq. 1) and EBI^2 (Eq. 4) are considered to evaluate the Drake caprock geomechanical properties (Fig. 6). The normalized Young's modulus (E) and Poisson's ratio (PR) based EBI^1 increases with increasing E and decreasing PR (Fig. 6a). However, Acoustic impedance (AI) and Deep resistivity (R_t) based EBI^2 do not follow the same linear trend. Instead, EBI^2 increases with increasing E, while very gentle changes occur in PR. Even the highest BI data cluster is not located within the lowest PR zone (Fig. 6b). BI range significantly varied between the studied methods, where most of the data points clustered in the lower region (between 0 to 0.5) in EBI^1. In EBI^2, most data points are clustered within the range between 0.25 and 0.75. When the BI from this study is compared with the background curves proposed by Perez and Marfurt (2014), a distinct dissimilarity is observed (Fig. 6). According to the Perez and Marfurt (2014) curves, most of the data points plot within the ductile to less-brittle region except for a few data points. Even the highest elastic BI clusters derived by both methods are away from the Perez and Marfurt (2014) curves. Based on EBI^2 brittleness range, a new templates (dotted lines in Fig. 6b) are proposed considering intervals 0.25. According to the proposed template, most of the studied data clustered between less-ductile to less-brittle regions. Considerable numbers of data points also fall within the brittle zone (BI > 0.75).

The well average BI maps reveal the lateral variation of the brittleness values which are illustrated in Fig. 7. Although the BI trend looks similar (low and high areas) between the methods, the range varied significantly, where EBI^1 ranges between 0.2 to 0.4 and 0.45 to 0.85 according to EBI^2 (Fig. 7). In terms of lateral variations, the BI trends also look similar (i.e., lateral variation) between both methods. Overall, higher brittleness is observed in EBI^2. In the north and west parts, the caprock shales are more brittle than in the southern part. Moreover, the lower Drake unit is more ductile than the upper Drake unit. Also, low BI values are observed below the oil/gas fields (e.g., Troll, Brage, Oseberg). In the proposed CO_2 injection site near the well 31/5-7 (red circle on the maps), both methods show that the lower Drake unit is relatively ductile than the upper Drake unit.

3.2. Seismic amplitude analysis

Average acoustic impedance (AI) map (Fig. 8a) of the primary caprock (Lower Drake unit) shows the AI ranges between 11000 to 6500 g/cm^3 x m/s. Low AI values are also observed underneath the oil/gas fields (i.e., Troll, Brage, Oseberg), similar to the brittleness maps (Fig. 7). Moreover, significantly low AI values have been seen in the southern part of the Tusse-Vette fault block. On the contrary, a high AI N-S trend following the Lomre Terrace is observed, extending up to the Brage Horst. In the vicinity of the possible CO_2 injection well, AI values exhibit an intermediate range compared to the other part of the study area. For detailed qualitative post-stacked seismic attributes analysis, a small 3D cropped volume from the survey GN01M1 has been used (Fig. 8b). This area is chosen considering well 31/5-7 (injection point) with possible plume migration to the north (the reservoir sandstone gently dipping towards south). The average AI values within this cropped area range between 9000 and 6500 g/cm^3 x m/s, significantly lower than the rest of the study area. Local variations are qualitatively evaluated by employing seismic attribute analysis in the later sub-sections.

3.2.1. Caprock and reservoir rock characterization

Seismic attribute-based characterization is carried out on the primary caprock shale (Lower Drake unit) and the reservoir sandstone (Johansen Formation). The average envelope attribute property of the lower Drake unit and the Johansen Formation, respectively, are shown in Fig. 9. Low envelope attribute, which is equivalent to low acoustic impedance contrast, illustrates cleaner clay or sand layers, while high values represent poorly sorted or vertical elastic property variations, which create high contrast acoustic impedance boundaries. There might be many other factors involved in characterizing caprock shales; however, the chosen properties are good tools for qualitative assessment. For instance, low values represent soft caprock, while the high values indicate stiff rocks. Moreover, when the envelope attribute shows low values, this represents higher porosity compared to the higher values within the reservoir unit.

The acoustic impedance contrast in caprock and reservoir zones ranges between 0 and 10000 g/cm^3 x m/s. A distinct soft low envelope NW-SE trend is observed within the lower Drake unit (Fig. 9a), which is also seen in the well average acoustic impedance map (Fig. 8a). However, the proposed injection well (31/5-7) is located relatively within the high impedance zone. On the contrary, the Johansen Formation within the study area represents overall clean sandstones with possible high porosity (assuming low contrast means high porosity), except for a few linear features (showing high impedance contrast). The injection well is located in one such elongated linear NW-SE oriented depositional feature (Fig. 9b)., The similarity between the well average and seismic attribute maps indicates the possibility of using seismic attributes for detailed rock properties analysis.

3.2.2. Faults and fractures

Variance attribute, which indicates the possible faults and fractures alignment, is demonstrated in Fig. 10. To evaluate the vertical continuity of faults and fractures, the top Johansen (reservoir sandstone), top lower Drake (caprock shale), and top Sognefjord (the reservoir of Troll field) surfaces are used. The faults and fractures identified on the top Sognefjord Formation look more prominent than the deeper surfaces might be due to seismic quality degradation with depth. The variance attribute clearly reveals the N-S-oriented major faults (Tusse, Svartlav, and Troll) and additional minor faults present in the area. The minor faults in the northern part, oriented in NW-SE direction, are also present in both the studied fault blocks (i.e., Tusse-Svartlav and Svartlav-Troll blocks). Another set of faults oriented in the NE-SW direction is located west of the injection well (31/5-7). The injection well is bounded by faults in the east and west directions. Considering the fault alignment and reservoir sandstone dip (dipping southward), the injected CO_2 plume might be migrated towards the north (red lines in Fig. 10) and

might accumulate near the Svartalv fault (SF). However, if the SF reactivates due to the CO_2 injection-induced fluid pressure increase, there might be a possibility of the CO_2 plume migration upward into the Sognefjord Formation (Fig. 10a). In such a scenario, the plume might migrate vertically (parallel to the fault plane) as well as laterally further north (upward direction).

3.3. Gas chimney in block 31/2

If the above-described faults reactivate due to injection-induced pressure increase, it might be used as a CO_2 plume migration path. The gas chimney parallels to a fault plane is a similar type of event that can be analyzed to understand the ultimate fate of CO_2 plume if a failure occurs. Fig. 11 represents a possible gas chimney in block 31/2, where the vertical disruption is observed on three seismic sections (Fig. 11b–d). This gas chimney is observed in the north of the Troll west gas field concentrated within the northern part of the Tusse fault (TF). Vertically this chimney started from the deeper section and ended in the Hordaland Clay Formation. High amplitude on top of the Hordaland Clay indicates possible gas leakage from the Troll reservoirs (i.e., Sognefjord and Fensfjord formations). Interpretation of the top Draupne Formation (primary caprock) demonstrates that the caprock shale was missing on top of the gas chimney area (Rahman et al., 2020). Also, several small-scale faults are present in the study area (Fig. 11b–d), where the high amplitude is also observed in the same overburden formation (i.e., Hordaland Clay). This indicates the leaking of small-scale faults as well (Fig. 11b). However, the amplitude is dimmer compared to the Tusse fault accumulation, suggesting that eventual leakages are less pronounced (Fig. 11b).

4. Discussion

4.1. Elastic brittleness indices

Brittleness template for the E-PR cross-plot adapted from Perez and Marfurt (2014) deviates considerably from the two estimated elastic property-based Brittleness Indices (EBI^1 & EBI^2) (Fig. 6). According to the template, most data points fall within the ductile to less-brittle zone, even with high Young's modulus values. There are no similarities in the brittleness increasing trend between the template and the methods used in this study. Perez and Marfurt (2014) template used in this study was estimated based on the Barnett Shale from the Fort Worth Basin, Texas, USA. A considerable deviation of brittleness indices value increasing trend is observed comparing the template with Drake Formation shale from the northern North Sea. One explanation might be the mineralogy and diagenetic differences between the Barnett and Drake shales. These dissimilarities indicate the need for basin-specific templates or even formation-specific templates if the formation differences are also substantial. This study stresses the necessity of future studies to establish a formation- or basin-specific rock physics templet to quantify the brittleness of the caprock shales in the Norwegian Continental Shelf (NCS). A new template is proposed based on the EBI^2 (Fig. 6b). The new template shows a deviation from the Perez and Marfurt (2014) curves and might be useful to assess the caprock brittleness indices property in the study area. However, the studied caprock's static Young's modulus range is considerably low compared to the mineral points, which needs to be addressed in the future to improve the template. Although this template needs further improvement, we suggest using this for caprock brittleness property evaluation in the Norwegian Continental Shelf (NCS) because the other template might mislead the caprock brittleness property assessment. Still, it is suggested to use Horsrud (2001) empirical equation when estimating static Young's modulus (E) to avoid the issue regarding the E property range.

Differences are also observed between EBI^1 and EBI^2, where the second method shows broader brittleness ranges, hence, representing brittleness indices with more resolution but the first method follows the Young's modulus trend better (Fig. 6). For instance, EBI^2 effectively delineates the temperature clusters with less-ductile and less-brittle to brittle zones (considering 0 to 0.25 as ductile and 0.75 to 1 as brittle) (Figs. 5e & 6b). Although the EBI^1 has a lower range of brittleness value, the normalized Young's modulus (E) and Poisson's ratio (PR) should have a better range. EBI^1 estimation equation (Eq-1) is proposed based on the Barnett Shale, which should not be treated as universal caprock but basin-specific. Therefore, the range needs to be updated based on local caprock properties, a similar approach to Rickman et al. (2008). Based on the five wells (30/9-29S, 31/1-1, 31/5-7, 31/7-1 & 31/2-19S) with measured shear velocity (V_s) data from the study area are used to define the minimum and maximum limit for E and PR for the Drake caprock shales. To avoid over and underestimation, P10 and P90 values have been used (Table 2). The lowest and highest values are used as the minimum and maximum static E (i.e., 2.43 and 6.68 GPa) and PR (i.e., 0.25 and 0.33) to update the EBI^1 maps for the upper and lower Drake units (Fig. 12). These maps represent broader ductility variability better than the maps created using the published data range (Figs. 7a & b). In the Aurora area, the lower Drake unit (primary caprock) shows relatively ductile, which is critical for the successful implementation of the Longship CCS project.

Table. 2
The ranges of static Young's modulus and Poisson's ratio of the upper and lower Drake units are estimated from five wells with measured V_s.

	E (GPa)			PR		
	P10	P50	P90	P10	P50	P90
Upper Drake	2.64	3.86	6.72	0.25	0.28	0.32
Lower Drake	2.25	3.69	6.58	0.27	0.31	0.34
All zones	2.43	3.80	6.68	0.25	0.29	0.33

4.2. Seal integrity and implication in CCS

Geomechanical properties can predict the level and type of deformation of any caprock under stress based on the brittleness indices (Nygård et al., 2006). Failure occurs quickly when the caprock is brittle, indicating less tolerance to significant strain. In comparison, ductile caprock shale has a higher tolerance to considerable strain and diffuses the deformation. The effect of burial depth on caprock brittleness is complicated and acts in both ways (i.e., both decreasing and increasing). For instance, an increase in depth leads to a rise in pressure and temperature; hence, increasing the degree of diagenesis by compaction processes (mechanical and chemical compactions) will increase the degree of stiffness. On the contrary, increasing temperature decreases rock stiffness. These opposite processes make it somewhat challenging to evaluate top seal effectiveness.

A wide range of elastic property-based brittleness indices (EBI) are observed within the Drake Formation (Fig. 6). The brittleness property of the studied shale formation varies from ductile to brittle. The studied wells exhibit a wide range of structural depth, explaining the diagenetic variation, which explains the variation of variable BI's. Stiff Drake caprock might be prone to shear failure or tensile fracture risk. However, in the Horda Platform area where the CO_2 injection well Eos (31/5-7) is located, the BI maps of the upper and lower Drake units (Figs. 7 & 12) show the presence of relatively ductile caprocks (low BI values). Although the upper Drake BI near the injection well is comparatively high, the primary caprock (lower Drake unit) represents a lower value near the injection location and also in the up-dip direction (i.e., north). 3D seismic attribute (envelope analysis) also reveals the local variation of acoustic impedance contrast (Fig. 9a); however, considering the whole study area, the acoustic impedance (AI) falls between the low to intermediate range (Fig. 8a). Considering the lower Drake thickness and low brittleness indices value near the CO_2 injection point, the caprock shale might be unlikely to be failed during injection in the Longship CCS project surrounding the well 31/5-7.

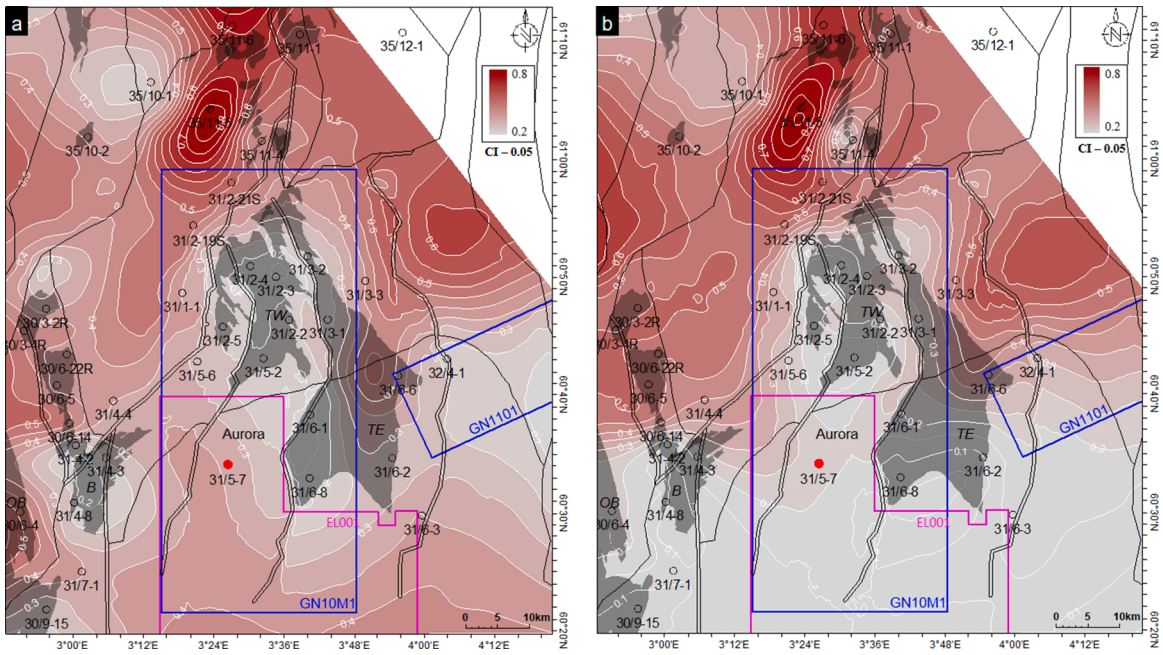

Fig. 12. Elastic property-based brittleness indices calculated using the new E and PR range which are estimated from the five measured Vs wells show the lateral variation of the upper (a) and lower (b) Drake units.

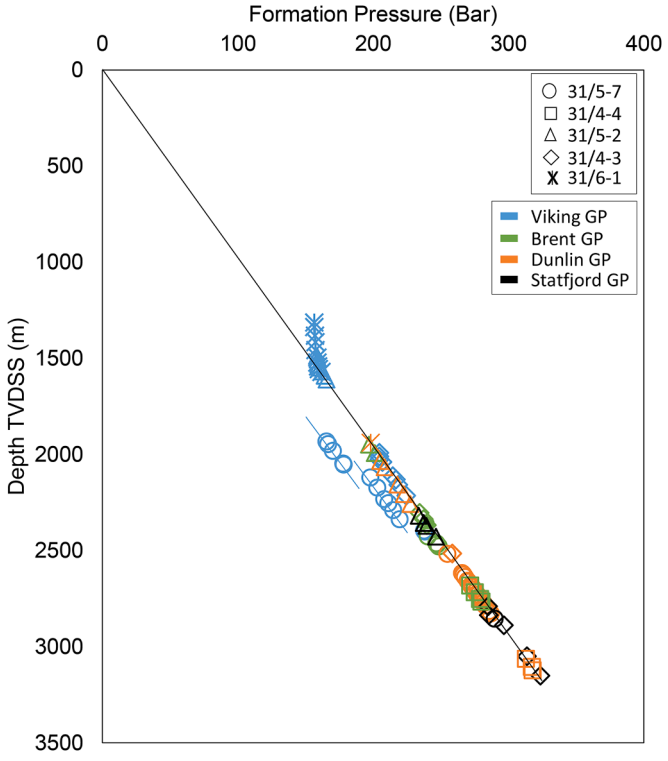

Fig. 13. Formation pressure extracted from NPD (2021) of 5 studied wells shows the pressure connectivity between different Groups. Note the depletion of the Viking group in the recently drilled well (31/5-7) due to production from the Troll Field.

A fault-related gas leakage might be a possible threat for CCS because the Aurora CO_2 reservoir is a fault-bounded structure. There might be the possibility of fault reactivation due to injection-related pressure changes. Although many faults are present near the injection area (Fig. 10), the formation pressure data from the Dunlin Group are unaffected by the Troll field production from the above strata, indicating sealed faults (Fig. 13). Moreover, the gas chimney identified in block 31/2 is located where the primary caprocks in the area (i.e., Draupne and Heather formations) are not present (Rahman et al., 2020; Fig. 11). This might be one of the reasons for the existence of the gas chimney triggering the fault to fail. However, this scenario with fault failure seems unlikely in the Aurora area because of a considerable thickness of ductile lower Drake caprock throughout the possible injection area. Moreover, formation pressures indicate no communication between the fault blocks in the present stress-state condition. However, the post-injection stress situation might be different; hence a fault seal analysis is needed to evaluate all possible sealing risks.

Although there is a correlation between elastic properties and seismic amplitude observed (Fig. 4c), the caprock sealing properties complex nature makes it challenging to quantify the sealing potential directly from seismic (Rahman et al., 2020). However, calibrating with wells, seismic attributes can reveal the relative lateral heterogeneity within the study area (Fig. 9). Different cementing processes in the chemical compaction realm further complicate the assessment of the effectiveness of top seal evaluation. Therefore, like this study, an integrated approach can significantly increase the confidence during the assessment of top seal integrity. In addition, the integrated workflow proposed in this study might be effective globally during caprock assessment for site-specific CCS projects because of the caprock shales' complex properties. However, this workflow does not consider any laboratory analysis (i.e., UCS, Triaxial test, etc.) and injection-induced stress-strain behavior of the caprock shales, which needs to be investigated before any injection decision makes for any CO_2 storage site.

5. Conclusions

Characterization of Drake caprock shale, mainly the lower Drake unit, is crucial for successful CO_2 storage in the Aurora injection site. This study introduced an integrated workflow to evaluate top seal properties and risk evaluation. The Drake caprock shale from the Aurora area is assessed as an example. The critical observations of this study are as follows:

- Although the upper Drake unit is more brittle than the lower unit, the Drake Formation caprock shale is relatively ductile.
- A new range for Drake Formation shale is proposed to normalize Young's modulus (E) and Poisson's ratio (PR) based brittleness indices estimation. The new range allows a broader BI distribution; hence, is suggested for NCS caprock characterization.
- An initial basin-specific caprock brittleness template for the E-PR cross plot has been proposed based on the EBI[2]. However, additional work is needed to improve this template, hence requiring awareness when used.
- Caprock quality in the Horda Platform area, specifically in and around the injection well (31/5-7), is relatively ductile compared to the north and northwest parts of the study area. Considering the long-term goal of the Longship CCS project, laboratory analysis should be carried out for a better understanding of the caprock.
- The formation pressure data and caprock thickness in the Aurora area reveal that it is improbable to have a top seal failure scenario in the present condition. However, the post-injection stress scenario needs to be evaluated for any possible sealing risks; hence, a coupled hydro-thermo-geomechanical flow simulation model should be carried out to assess the risks.
- Considering the complex nature of caprock shale properties, the integrated methods used in this study have shown to be useful and viable in assessing the overall top seal geomechanical properties and integrity. Moreover, irrespective of limitations, the flexibility of the workflow indicates the feasibility of using this approach globally.

Considering all the caprock assessment methods presented in this study, we conclude that the top seal at the proposed Aurora site is favorable for CO_2 storage.

CRediT authorship contribution statement

Md Jamilur Rahman: Conceptualization, Methodology, Formal analysis, Investigation, Writing – original draft, Writing – review & editing, Visualization. **Manzar Fawad:** Writing – review & editing, Supervision. **Jens Jahren:** Writing – review & editing, Supervision. **Nazmul Haque Mondol:** Writing – review & editing, Supervision, Project administration, Funding acquisition.

Declaration of Competing Interest

The authors declare that they have no known competing financial interests or personal relationships that could have appeared to influence the work reported in this paper.

Acknowledgments

We are grateful for the financial support of the Research Council of Norway for the OASIS (Overburden Analysis and Seal Integrity Study for CO_2 Sequestration in the North Sea) project (NFR-CLIMIT project #280472). We are indebted to the additional funding and data provided by Norwegian Petroleum Directorate (NPD), Gassnova, Equinor, and TotalEnergies. Lloyd's Register provides academic software licenses for Interactive Petrophysics and Schlumberger for Petrel.

References

Baig, I., Faleide, J.I., Mondol, N.H., Jahren, J., 2019. Burial and exhumation history controls on shale compaction and thermal maturity along the Norwegian North Sea basin margin areas. Mar. Pet. Geol. 104, 61–85. https://doi.org/10.1016/j.marpetgeo.2019.03.010.

Barnes, A.E., 1991. Instantaneous frequency and amplitude at the envelope peak of a constant-phase wavelet. Geophysics 56, 1058–1060. https://doi.org/10.1190/1.1443115.

Bjørlykke, K., Høeg, K., Mondol, N.H., 2015. Introduction to geomechanics: stress and strain in sedimentary basins. Petroleum Geoscience. Springer, pp. 301–318. https://doi.org/10.1007/978-3-642-34132-8.

Bjørlykke, K., Line, line H., Jahren, J., Mondol, N.H., Aagaard, P., Hellevang, H., 2017. Compaction of sand and clay - constraints from experimental compaction, chemical reactions and fluid flow during burial–an overview. AAPG Annual Convention and Exhibition. AAPG, Houston, Texas.

Chen*, J., Zhang, G., Chen, H., Yin, X., 2014. The construction of shale rock physics effective model and prediction of rock brittleness. In: Proceedings of the SEG Technical Program Expanded Abstracts. Society of Exploration Geophysicists, pp. 2861–2865. https://doi.org/10.1190/segam2014-0716.1.

Chen, T., Feng, X.T., Cui, G., Tan, Y., Pan, Z., 2019. Experimental study of permeability change of organic-rich gas shales under high effective stress. J. Nat. Gas Sci. Eng. 64, 1–14. https://doi.org/10.1016/j.jngse.2019.01.014.

Chiaramonte, L., White, J.A., Trainor-Guitton, W., 2015. Probabilistic geomechanical analysis of compartmentalization at the Snøhvit CO2 sequestration project. J. Geophys. Res. Solid Earth 120, 1195–1209.

Chopra, S., Marfurt, K.J., 2005. Seismic attributes—a historical perspective. Geophysics 70, 3SO–28SO. https://doi.org/10.1190/1.2098670.

Cohen, L., 1995. Time-Frequency Analysis. Prentice Hall PTR, Englewood Cliffs, NJ.

Færseth, R.B., 1996. Interaction of Permo-Triassic and Jurassic extensional fault-blocks during the development of the northern North Sea. J. Geol. Soc. Lond. 153, 931–944. https://doi.org/10.1144/gsjgs.153.6.0931.

Fawad, M., Mondol, M.N.H., 2021. Method for estimating rock brittleness from well-log data Patent application (application #20191505 issued - December 30, 2019; granted – August 08, 2021) 345798, B1. https://search.patentstyret.no/Patentskrifter/Publisering/345798.pdf.

Gale, J.F.W., Reed, R.M., Holder, J., 2007. Natural fractures in the Barnett Shale and their importance for hydraulic fracture treatments. Am. Assoc. Pet. Geol. Bull. 91, 603–622. https://doi.org/10.1306/11010606061.

Grieser, W.V., Bray, J.M., 2007. Identification of production potential in unconventional reservoirs. In: Proceedings of the Production and Operations Symposium. Society of Petroleum Engineers. https://doi.org/10.2118/106623-MS.

Guo, Z., Chapman, M., Li, X., 2012. Exploring the effect of fractures and microstructure on brittleness index in the Barnett Shale. In: Proceedings of the SEG Technical Program Expanded Abstracts. Society of Exploration Geophysicists, pp. 1–5. https://doi.org/10.1190/segam2012-0771.1.

Handin, J., Hager, R.V, 1957. Experimental deformation of sedimentary rocks under confining pressure: tests at room temperature on dry samples. Am. Assoc. Pet. Geol. Bull. 41, 1–50. https://doi.org/10.1306/5CEAE5FB-16BB-11D7-8645000102C1865D.

Handin, J., Hager, R.V, Friedman, M., Feather, J.N., 1963. Experimental deformation of sedimentary rocks under confining pressure: pore pressure tests. Am. Assoc. Pet. Geol. Bull. 47, 717–755.

Hansen, J.A., Mondol, N.H., Tsikalas, F., Faleide, J.I., 2020. Caprock characterization of upper Jurassic organic-rich shales using acoustic properties, Norwegian Continental Shelf. Mar. Pet. Geol. 121, 104603 https://doi.org/10.1016/j.marpetgeo.2020.104603.

Hart, B.S., Macquaker, J.H.S., Taylor, K.G., 2013. Mudstone ("shale") depositional and diagenetic processes: implications for seismic analyses of source-rock reservoirs. Interpretation 1, B7–B26. https://doi.org/10.1190/INT-2013-0003.1.

Herwanger, J.V, Bottrill, A.D., Mildren, S.D., 2015. Uses and abuses of the brittleness index with applications to hydraulic stimulation. In: Proceedings of the Unconventional Resources Technology Conference. Society of Exploration Geophysicists, American Association of Petroleum Geologists, San Antonio, Texas, pp. 1215–1223. https://doi.org/10.15530/urtec-2015-2172545, 20-22 July 2015.

Holt, R.M., Fjaer, E., Nes, O.M., Alassi, H.T., 2011. A shaly look at brittleness. In: Proceedings of the 45th US Rock Mechanics/Geomechanics Symposium. American Rock Mechanics Association.

Holt, R.M., Fjær, E., Stenebråten, J.F., Nes, O.M., 2015. Brittleness of shales: relevance to borehole collapse and hydraulic fracturing. J. Pet. Sci. Eng. 131, 200–209. https://doi.org/10.1016/j.petrol.2015.04.006.

Horsrud, P., 2001. Estimating mechanical properties of shale from empirical correlations. SPE Drill. Complet. 16, 68–73.

Husmo, T., Hamar, G.P., Høiland, O., Johannesen, E.P., Rømuld, A., Spencer, A.M., Titterton, R., 2003. Lower and middle jurassic. In: Evans, D., Graham, C., Armour, A., Bathurst, P. (Eds.), The Millennium Atlas: Petroleum Geology of the Central and Northern North Sea. The Geological Society, London, UK, pp. 129–155.

Ingram, G.M., Urai, J.L., Naylor, M.A., 1997. Sealing processes and top seal assessment. Norwegian Petroleum Society Special Publications. Elsevier, pp. 165–174. https://doi.org/10.1016/S0928-8937(97)80014-8.

Jin, X., Shah, S.N., Roegiers, J.-C., Zhang, B., 2014. Fracability evaluation in shale reservoirs-an integrated petrophysics and geomechanics approach. In: Proceedings of the SPE Hydraulic Fracturing Technology Conference. Society of Petroleum Engineers. https://doi.org/10.2118/168589-MS.

Johnson, J.R., Hansen, J.A., Rahman, M.D.J., Renard, F., Mondol, N.H., 2022. Mapping the maturity of organic-rich shale with combined geochemical and geophysical data, Draupne Formation, Norwegian Continental Shelf. Mar. Pet. Geol., 105525

Josh, M., Esteban, L., Delle Piane, C., Sarout, J., Dewhurst, D.N., Clennell, M.B., 2012. Laboratory characterisation of shale properties. J. Pet. Sci. Eng. 88-89, 107–124. https://doi.org/10.1016/j.petrol.2012.01.023.

Kivi, I.R., Ameri, M., Molladavoodi, H., 2018. Shale brittleness evaluation based on energy balance analysis of stress-strain curves. J. Pet. Sci. Eng. 167, 1–19. https://doi.org/10.1016/j.petrol.2018.03.061.

Liu, B., Yang, Y., Li, Jiangtao, Chi, Y., Li, Junhui, Fu, X., 2020. Stress sensitivity of tight reservoirs and its effect on oil saturation: a case study of lower cretaceous tight clastic reservoirs in the Hailar Basin, Northeast China. J. Pet. Sci. Eng. 184, 106484 https://doi.org/10.1016/j.petrol.2019.106484.

Longship-Report, 2020. Longship - carbon capture and storage.

Marion, D., Nur, A., Yin, H., Han, D.-H., 1992. Compressional velocity and porosity in sand-clay mixtures. Geophysics 57, 554–563. https://doi.org/10.1190/1.1443269.
Mondol, N.H., Grande, L., Bjørnarå, T.I., Thompson, N., 2022. Caprock characterization of the northern lights co_2 storage project, offshore Norway. In: Proceedings of the EAGE GeoTech 2022 Sixth EAGE Workshop on CO_2 Geological Storage. European Association of Geoscientists & Engineers, pp. 1–5.
Mondol, N.H., 2018. Seal quality prediction using E-Poisson's ratio rock physics templet – a case study from the Norwegian Barents Sea. In: Proceedings of the Geo Convention. May 7-11, Calgary, Canada, 2018.
Mondol, N.H., Bjørlykke, K., Jahren, J., Høeg, K., 2007. Experimental mechanical compaction of clay mineral aggregates—changes in physical properties of mudstones during burial. Mar. Pet. Geol. 24, 289–311. https://doi.org/10.1016/j.marpetgeo.2007.03.006.
Northern Lights [WWW Document], 2022 n.d. URL https://northernlightsccs.com/what-we-do/.
NPD,NPD FactPages [WWW Document]. 2021. URL https://npdfactpages.npd.no/factpages/Default.aspx?culture=en (last access: June 2021).
Nygård, R., Gutierrez, M., Bratli, R.K., Høeg, K., 2006. Brittle–ductile transition, shear failure and leakage in shales and mudrocks. Mar. Pet. Geol. 23, 201–212. https://doi.org/10.1016/j.marpetgeo.2005.10.001.
Pablo, B.A., 2004. Acoustic impedance inversion of the Lower Permian carbonate buildups in the Permian Basin, Texas. https://hdl.handle.net/1969.1/1068.
Park, J.-W., Guglielmi, Y., Graupner, B., Rutqvist, J., Kim, T., Park, E.-S., Lee, C., 2020. Modeling of fluid injection-induced fault reactivation using coupled fluid flow and mechanical interface model. Int. J. Rock Mech. Min. Sci. 132, 104373.
Partington, M.A., Copestake, P., Mitchener, B.C., Underhill, J.R., 1993. Biostratigraphic calibration of genetic stratigraphic sequences in the Jurassic-lowermost Cretaceous (Hettangian to Ryazanian) of the North Sea and adjacent areas. In: Parker, J.R. (Ed.), Proceedings of the Petroleum Geology of Northwest Europe: Proceedings 4th Conference London (1992). Geological Society of London, UK, pp. 371–386. https://doi.org/10.1144/0040371.
Perez Altamar, R., Marfurt, K., 2014. Mineralogy-based brittleness prediction from surface seismic data: application to the Barnett shale. Interpretation 2, T1–T17. https://doi.org/10.1190/INT-2013-0161.1.
Peters, G., Sognnæs, I., 2019. The role of carbon capture and storage in the mitigation of climate change. CICERO Rep.
Rahman, M.J., Fawad, M., Jahren, J., Mondol, N.H., 2022. Influence of depositional and diagenetic processes on Caprock properties of CO_2 Storage Sites in the Northern North Sea, Offshore Norway. Geosciences. https://doi.org/10.3390/geosciences12050181.
Rahman, M.J., Choi, J.C., Fawad, M., Mondol, N.H., 2021. Probabilistic analysis of Vette fault stability in potential CO_2 storage site Smeaheia, offshore Norway. Int. J. Greenh. Gas Control 108, 103315. https://doi.org/10.1016/j.ijggc.2021.103315.
Rahman, M.J., Fawad, M., Mondol, N.H., 2020. Organic-rich shale caprock properties of potential CO_2 storage sites in the northern North Sea, offshore Norway. Mar. Pet. Geol. 122, 104665 https://doi.org/10.1016/j.marpetgeo.2020.104665.
Rickman, R., Mullen, M.J., Petre, J.E., Grieser, W.V., Kundert, D., 2008. A practical use of shale petrophysics for stimulation design optimization: all shale plays are not clones of the Barnett shale. In: Proceedings of the SPE Annual Technical Conference and Exhibition. Society of Petroleum Engineers. https://doi.org/10.2118/115258-MS.
Rogelj, J., Shindell, D., Jiang, K., Fifita, S., Forster, P., Ginzburg, V., Handa, C., Kheshgi, H., Kobayashi, S., Kriegler, E., 2018. Mitigation pathways compatible with 1.5 C in the context of sustainable development, in: global warming of 1.5°C. Intergovernmental Panel on Climate Change 93–174.
Rutqvist, J., Birkholzer, J., Cappa, F., Tsang, C.F., 2007. Estimating maximum sustainable injection pressure during geological sequestration of CO_2 using coupled fluid flow and geomechanical fault-slip analysis. Energy Convers. Manag. 48, 1798–1807.
Rybacki, E., Meier, T., Dresen, G., 2016. What controls the mechanical properties of shale rocks?–Part II: Brittleness. J. Pet. Sci. Eng. 144, 39–58. https://doi.org/10.1016/j.petrol.2016.02.022.
Sharma, R.K., Chopra, S., 2012. New attribute for determination of lithology and brittleness. In: Proceedings of the SEG Technical Program Expanded Abstracts 2012. Society of Exploration Geophysicists, pp. 1–5. https://doi.org/10.1190/segam2012-1389.1.
Skurtveit, E., Choi, J.C., Osmond, J., Mulrooney, M., Braathen, A., 2018. 3D fault integrity screening for Smeaheia CO_2 injection site. In: Proceedings of the 14th Greenhouse Gas Control Technologies Conference Melbourne, pp. 21–26.
Steel, R., Ryseth, A., 1990. The Triassic—Early Jurassic succession in the northern North Sea: megasequence stratigraphy and intra-Triassic tectonics. Geol. Soc. London, Spec. Publ. 55, 139–168. https://doi.org/10.1144/GSL.SP.1990.055.01.07.
Steel, R.J., 1993. Triassic–Jurassic megasequence stratigraphy in the Northern North Sea: rift to post-rift evolution. In: Proceedings of the Geological Society, London, Petroleum Geology Conference Series. Geological Society of London, pp. 299–315. https://doi.org/10.1144/0040299.
Storvoll, V., Bjørlykke, K., Mondol, N.H., 2005. Velocity-depth trends in Mesozoic and Cenozoic sediments from the Norwegian Shelf. Am. Assoc. Pet. Geol. Bull. 89, 359–381. https://doi.org/10.1306/10150404033.
Tan, Y., Pan, Z., Feng, X.T., Zhang, D., Connell, L.D., Li, S., 2019. Laboratory characterisation of fracture compressibility for coal and shale gas reservoir rocks: a review. Int. J. Coal Geol. 204, 1–17. https://doi.org/10.1016/j.coal.2019.01.010.
Taner, M.T., 2001. Seismic attributes. CSEG Rec 26, 49–56.
Walles, F., 2004. A new method to help identify unconventional targets for exploration and development through integrative analysis of clastic rock property fields.
Wang, F.P., Gale, J.F.W., 2009. Screening criteria for shale-gas systems.
Yang, Y., Sone, H., Hows, A., Zoback, M.D., 2013. Comparison of brittleness indices in organic-rich shale formations. In: Proceedings of the 47th US Rock Mechanics/Geomechanics Symposium. American Rock Mechanics Association.
Zhang, D., Ranjith, P.G., Perera, M.S.A., 2016. The brittleness indices used in rock mechanics and their application in shale hydraulic fracturing: a review. J. Pet. Sci. Eng. 143, 158–170. https://doi.org/10.1016/j.petrol.2016.02.011.